ACS OMEGA

http://pubs.acs.org/journal/acsodf

Article

Simultaneous Quantitation of Lead and Cadmium on an EDTA-Reduced Graphene Oxide-Modified Glassy Carbon Electrode

Nishanthi Vasanthi Sridharan and Badal Kumar Mandal*

Cite This: ACS Omega 2022, 7, 45469−45480

Read Online

ACCESS | Metrics & More | Article Recommendations | Supporting Information

ABSTRACT: Cadmium (Cd) and lead (Pb) are classified as category one toxicants. The provisional guideline values, according to the World Health Organization (WHO), for Cd and Pb are 3 and 10 ppb, respectively. An easy, quick, and cheap analytical technique is in demand for the determination of these toxic heavy metals in water. Hence, a novel electrochemical sensing platform is developed by modifying the glassy carbon electrode with ethylenediaminetetraacetic acid (EDTA)-functionalized reduced graphene oxide (ErGO) for the low-cost simultaneous quantitation of toxic heavy-metal ions, lead and cadmium, in real water samples. EDTA is grafted to the surface of graphene oxide, via amine linkage, and the oxygen functionality is reduced by a green agent, tyrosine. Various physical and electrochemical characterizations of the as-prepared electrocatalytic material were performed by X-ray diffraction (XRD), Fourier transform infrared (FTIR) spectroscopy, thermogravimetric analysis (TGA), ζ-potential, ultraviolet diffuse reflectance spectroscopy (UV-DRS), cyclic voltammetry (CV), electrochemical impedance spectroscopy (EIS), etc. The glassy carbon electrode (GCE) is modified with ErGO by a simple drop-casting method for simultaneous metal-ion quantitation by differential pulse voltammetry (DPV). EDTA functionalization of graphene oxide and its further reduction using the green agent enhance the stability and sensitivity of the electrode substrate. The limits of detection for cadmium and lead ions calculated for ErGO/GCE are 1.02 and 2.52 ppb, while the limits of quantification for lead and cadmium ions are 3.41 and 8.4 ppb, and their sensitivities are 0.8 and 0.6 nA/ppb, respectively. Real river water contains 200.2 ± 0.38 ppb of Pb^{2+} ions (mean ± stdev, n = 3) by the DPV technique, which is validated by ICP-OES analysis.

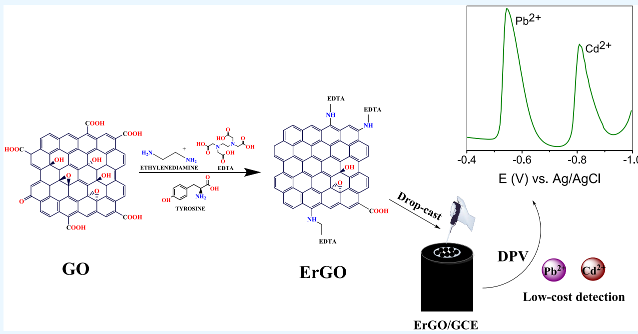

1. INTRODUCTION

Harmful chemical components, bio-wastes, and other pollutants have been incessantly contaminating surface water sources over the past decade due to rapid industrialization and anthropogenic activities. Among them, heavy-metal ions (HMIs) are a huge threat to the environment.[1] The toxic HMIs such as lead, cadmium, chromium, mercury, and arsenic are present in water at more than the permitted levels of 10 and 3 ppb for lead and cadmium set by the World Health Organization (WHO).[2] Lead and cadmium are ranked among the top 10 under ATSDR 2019 substance priority list. The main sources of lead and cadmium in environmental samples are burning fossil fuels, mining, paints and ceramic products, coal and mineral fertilizers, production of batteries and other metals like Zn, Cu, etc. Exposure to these heavy metals causes oxidative damage due to toxic mechanistic actions of these metal-induced reactive oxygen species (ROS) generation resulting in damage to tissues, DNA repair, and cancer in humans and animals.[3,4] The impact is synergistically adverse when they occur as mixtures, like individual ions in environmental samples. Therefore, simultaneous detection and quantitation of multiple toxic analytes is of utmost importance in the present-day scenario.[5]

Although other techniques, such as inductively coupled plasma-optical emission spectrometry (ICP-OES), inductively coupled plasma-mass spectrometry (ICP-MS), atomic absorption (AAS) and atomic emission spectrophotometry (AES), mass spectrometry (MS), and high-performance liquid chromatography (HPLC) offer high resolution and sensitivity, voltammetry techniques are preferred for its portability, accuracy, and easy and cost-effective methodology.[6] Differential pulse voltammetry is one of the most sensitive voltammetry techniques.[7] In recent times, graphene-modified electrodes have drawn attention for heavy-metal-ion detection due to their high sensitivity and accuracy.[8]

Materials with a controllable structure and size, high porosity, large electroactive area, and low charge-transfer resistance are desirable for electrode modification to enhance

Received: September 20, 2022
Accepted: November 24, 2022
Published: December 2, 2022

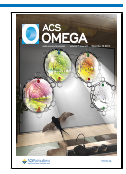

Scheme 1. Chelation Mechanism of Target Metal Ions with the COO^- Group of EDTA

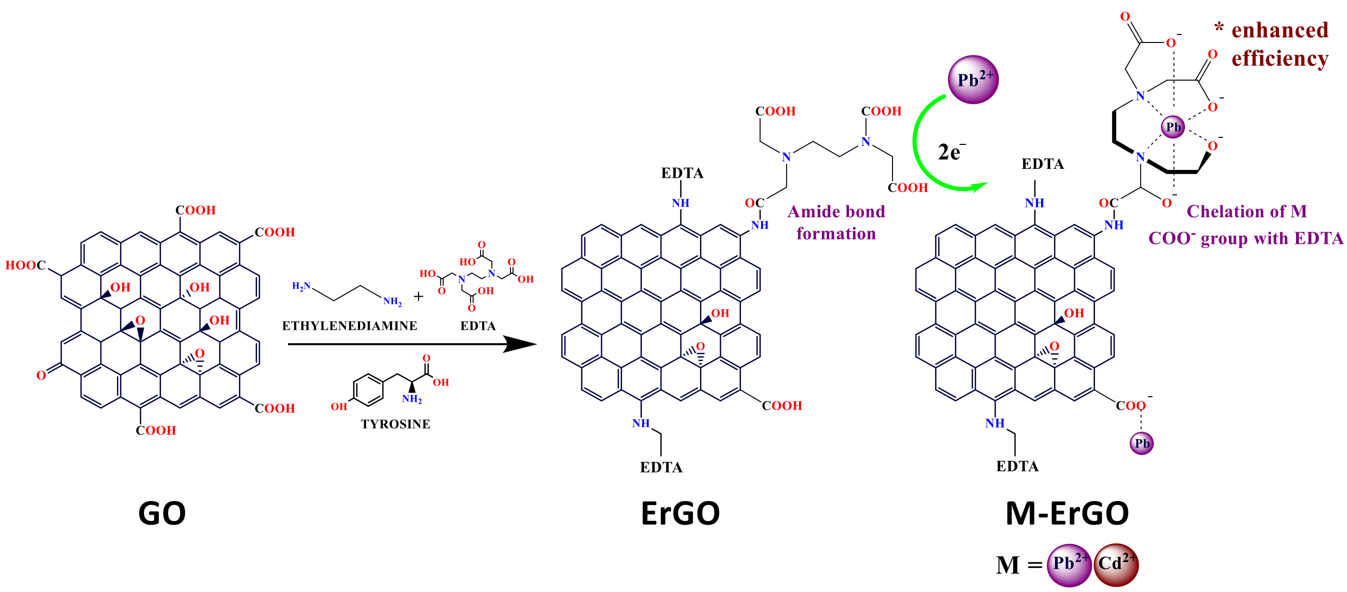

sensitivity.[9] Also, the material should be able to detect trace-level quantities with ultrasensitivity, good selectivity, repeatability and stability, and lower limits of detection.[10]

Graphene-based nanomaterials are a great choice for electrochemical detection because of their conductivity and good electron transfer behavior.[11,12] Graphene oxide (GO) is the oxidized form of graphene with various oxygen functionalities such as hydroxy, epoxy, carbonyl, and carboxyl groups present on their basal planes and edges, respectively.[13] Functionalized reduced graphene oxide is of much interest where the functionalizing agent-specific interaction of the functional site plays an essential role in the selectivity of the analyte.[14] Generally, covalent functionalization through chemical methods is an economic and effective way of protection strategies of two-dimensional (2D) materials for stability, excellent surface activity, and biocompatibility.[15,16]

To enhance sensitivity, ethylenediaminetetraacetic acid (EDTA) has been used to functionalize GO by grafting via an amine linkage in the present work (Scheme 1). EDTA is a hexadentate chelating ligand that binds to the metal ion to form a complex. On the other hand, tyrosine, a biomaterial, is used for the reduction of EDTA-functionalized GO to enhance stability further. The nitrogen-containing groups contribute to the stability and chelating factors of the material for its effective performance. The stability of the material is also contributed by the covalent amine linkage between the EDTA groups and rGO. A lot of efforts have been made earlier to synthesize EDTA-based graphene composites through chemical methods such as silanization,[17] solvothermal,[18] hydrothermal[19] methods, etc. These materials have been widely used in the adsorption of metal ions[20−23] and organic pollutants.[24−27] The EDTA-modified electrodes[28,29] and their composites on graphene[30,31] and polymer[32] supports have been used for electrochemical sensing of various analytes.[33] It has been reported that EDTA significantly increased the sensitivity due to its strong binding ability with metals, as well as improved selectivity, stability, and reproducibility.[34] The selectivity of the EDTA group depends on the pH of the analyte solution. In this work, all analyses, including real sample analysis, have been done at the original pH values.

The physiochemical characterization and functionalization of the materials were confirmed by X-ray diffraction (XRD), Fourier transform infrared (FTIR) spectroscopy, thermogravimetric analysis (TGA), ζ-potential studies, ultraviolet diffuse reflectance spectroscopy (UV-DRS), scanning electron microscopy (SEM), and field-emission scanning electron microscopy (FESEM). The electroanalytical measurements have been carried out by cyclic voltammetry (CV), electrochemical impedance spectroscopy (EIS), and simultaneous quantitation of metal ions by the differential pulse voltammetry (DPV) method.

For the detection of heavy-metal ions and their interference studies, the glassy carbon electrode (GCE) is used because of its large potential window, ease of surface modification, and the highly conductive surface. Surface modification was done by a simple drop-casting method over GCE where the prepared electrocatalyst material was coated and air-dried for all electrochemical experiments. The $\pi-\pi$ interaction of the materials with the electrode surface is aided by performing at least 20 segments of cyclic voltammetry at a scan rate of 50 mV/s. No additional binders have been used in this work.

In this paper, EDTA-functionalized GO was synthesized by chemical functionalization followed by a green reduction technique, devoted to a low-cost voltammetric quantitation of simultaneous Pb^{2+} and Cd^{2+} ions in the water samples collected from the River Palar, Vellore. The electrochemical performance of the material is due to both EDTA and rGO. To our knowledge, this is the first report of green-reduced EDTA-functionalized GO (ErGO) for simultaneous quantitation of heavy-metal ions by the DPV technique.

2. EXPERIMENTAL SECTION

2.1. Chemicals and Reagents. Graphite flakes, sodium nitrate ($NaNO_3$), potassium permanganate ($KMnO_4$), concentrated sulfuric acid (H_2SO_4, 98%), hydrogen peroxide (H_2O_2, 30%), ethylenediamine, ethylenediaminetetraacetic acid (EDTA), *N*-methyl-2-pyrrolidone (NMP), and L-tyrosine were used for the synthesis of the material. Ethanol, potassium ferricyanide, potassium chloride, sulfuric acid, potassium dihydrogen phosphate, disodium phosphate for phosphate

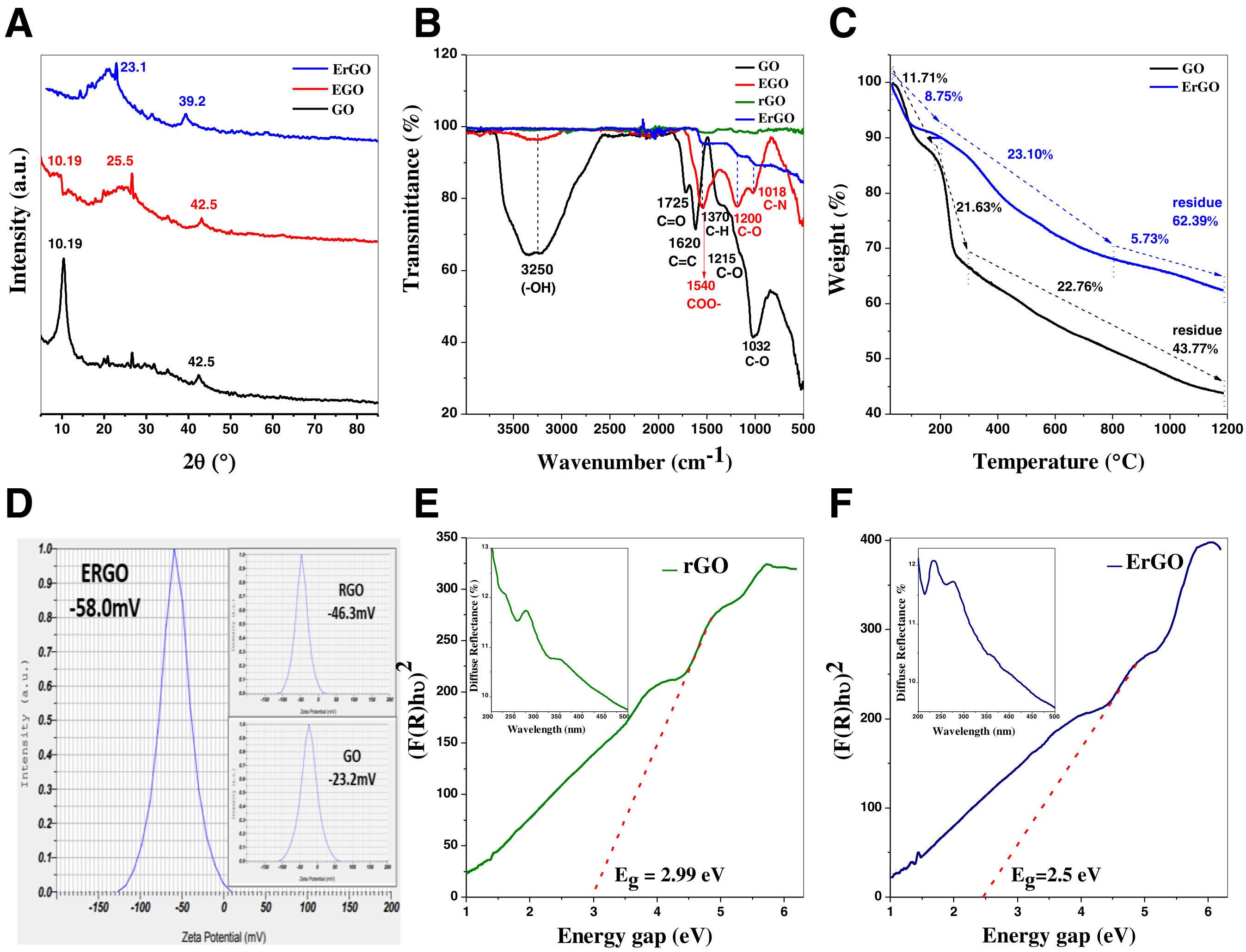

Figure 1. Physicochemical characterization of the synthesized GO, rGO, and ErGO materials: (A) XRD, (B) FTIR, (C) TGA, (D) ζ potential studies, and (E, F) UV-DRS spectrum.

buffer, anhydrous sodium acetate and glacial acetic acid for sodium acetate buffer, lead acetate, and cadmium acetate were used for the electrochemical studies. Mercury (II) chloride, magnesium (II) acetate, zinc (II) acetate, nickel (II) nitrate, cobalt (II) acetate, copper (II) acetate, and iron (II) nitrate were used for interference studies. All materials were purchased from Merck and Sigma-Aldrich.

2.2. Instrumentation. CV, EIS, and DPV studies were carried out using the electrochemical workstation (model CHI660C, CH Instruments). The characterizations of the materials GO, rGO, and ErGO were analyzed using a Powder XRD (Model Bruker D8 Advance), FTIR spectrophotometer (Model Shimadzu IR Affinity-1), TA instruments (Model SDT Q600), Nanosizer (Model Horiba Scientific, SZ 100), UV–visible spectrophotometer JASCO (V-670 PC), SEM (Model Carl Zeiss EVO/18 Research), FESEM (Thermo Fisher FEI QUANTA 250 FEG), and Avio 200 ICP-OES (Perkin Elmer).

2.3. Synthesis of EDTA-Functionalized rGO. GO was synthesized by modified Hummer's method through the oxidation of graphite.[35] Briefly, 2 g of graphite flakes, 2 g of sodium nitrate, and 90 mL of concentrated sulfuric acid were stirred in an ice bath. $KMnO_4$ was added as an oxidizing agent to the suspension very slowly and stirred for 4 h while the reaction temperature was maintained below 15 °C. A pasty brownish suspension was diluted by slow addition of distilled water under vigorous stirring at room temperature. After 2 h, the mixture was refluxed at 98 °C for 15 min and the temperature was then changed to 30 °C, which gave a brown-colored solution. It was then finally treated with 40 mL of 30% H_2O_2 to remove any unreacted ions. The resulting yellowish-brown mixture was washed repeatedly using 10% HCl and distilled water several times until the gel was formed and a neutral pH was obtained. The final product was dried in a hot air oven at 60 °C to obtain GO.[36]

GO was functionalized with EDTA through an amine linkage. EDTA-functionalized GO was synthesized based on a reported method after some modifications.[37] Briefly, GO dispersion in ethylenediamine was sonicated and then stirred at 50 °C. EDTA aqueous solution was added to the amine-functionalized GO dispersion and the resulting mixture was refluxed at 80°, for 24 h. The black suspension was centrifuged and washed with distilled water. The product was dried in a hot air oven at 60 °C to obtain EDTA-functionalized graphene oxide (EGO).

EGO was reduced using tyrosine, a bio-reductant and stabilizing agent based on a reported method by our group.[38] Then, 50 mL of EGO (1 mg/L) dispersion was treated with 500 mg of tyrosine. Ammonia solution was added to maintain

https://doi.org/10.1021/acsomega.2c06080
ACS Omega 2022, 7, 45469−45480

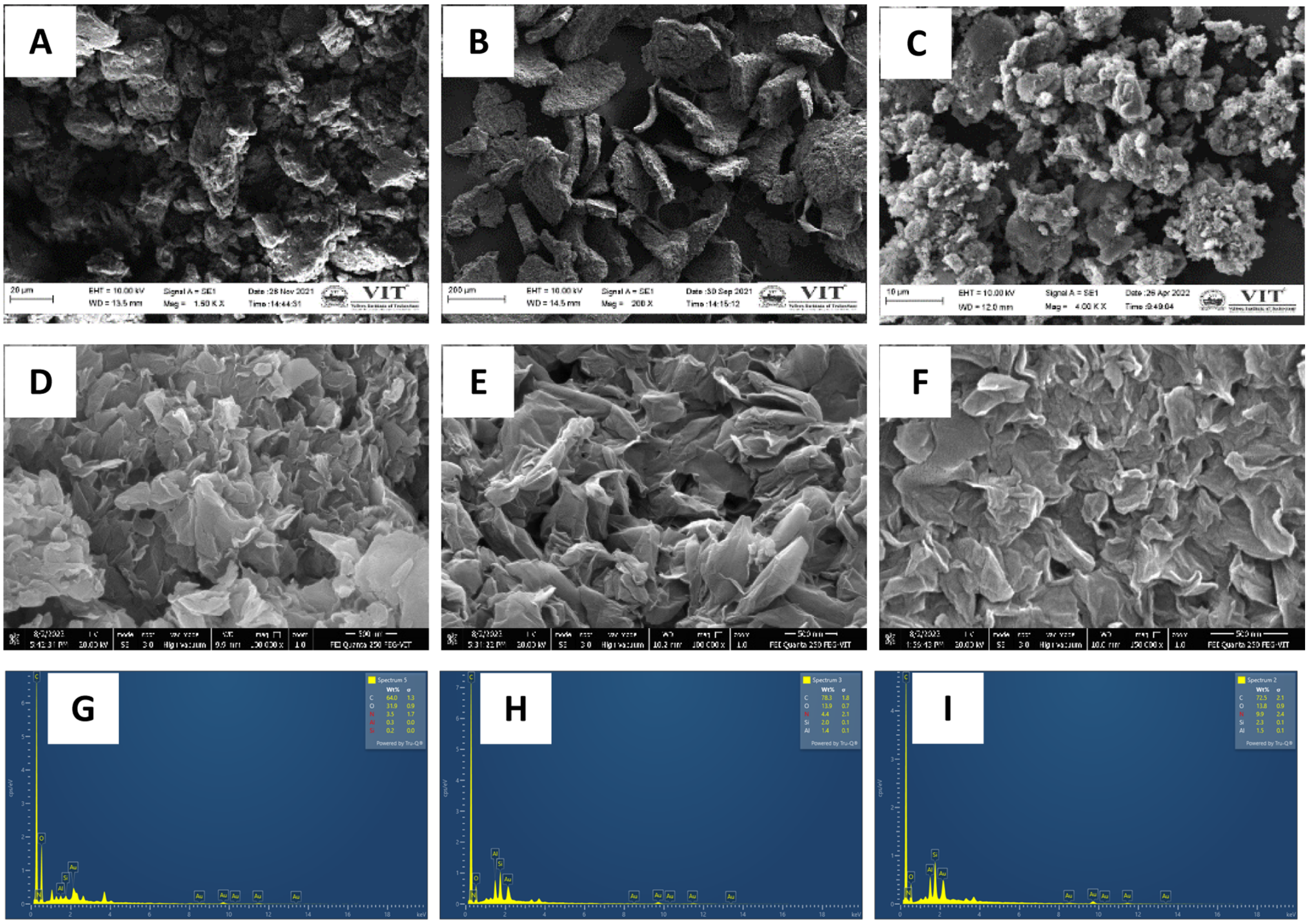

Figure 2. Microscopic study of the synthesized nanomaterials: (A−C) SEM images, (D−F) FESEM images, and (G−I) EDAX spectra of GO, rGO, and ErGO, respectively.

pH at 12. The reaction mixture was refluxed at 100 °C in an oil bath for about 8 h. The black suspension was centrifuged and washed with ethanol and distilled water several times. The final product was dried in a hot air oven at 80 °C to obtain EDTA-functionalized reduced graphene oxide (ErGO). rGO was also synthesized from GO following the same reduction method.[38] The electrochemical performances of the as-synthesized rGO and ErGO materials are compared using CV and EIS.

2.4. Preparation of the Electrode. The electrochemical studies were carried out using a three-electrode system, consisting of a modified glassy carbon working electrode, an Ag/AgCl reference electrode, and a platinum wire counter electrode. The ErGO material (1 mg) was dispersed in 1000 μL of ethanol by sonication for 2 min before coating on the electrode surface. The modification of GCE was done by drop-casting the ErGO dispersion. The electrode was then air-dried and the modified electrode was represented as ErGO/GCE. The rGO/GCE was also prepared by a similar method.

2.5. Preparation of Real Samples. The real water sample collected from a nearby river water source was centrifuged and filtered to remove any solid impurities. The pH of the water sample was kept original. DPV measurements were done for river water and samples spiked with 10, 20, and 30 ppm by the standard addition method.[39,40]

3. RESULTS AND DISCUSSION

3.1. Characterization of GO, rGO, and ErGO Materials. The physiochemical characterization of the synthesized materials was done by XRD, FTIR, TGA, Raman, and ζ-potential studies (Figure 1). The X-ray diffraction patterns of GO and ErGO reveal changes in the structure in functionalization and reduction (Figure 1A). The sharp diffraction peak at 2Θ of 10.26° confirms the formation of GO. After functionalization and reduction, the peak is shifted to 2Θ of 23° due to a decrease in interlayer spacing and exfoliation of the crystalline structure.

The functionalizing groups on the surface of GO were further confirmed by FTIR analysis (Figure 1B). The characteristic peaks for the oxygen functional groups of GO are observed at 3250 cm^{-1} (−OH), 1725 cm^{-1} (C═O stretching in COOH), 1620 cm^{-1} (C═C stretching in the aromatic ring), 1370 cm^{-1} (C−H stretching), 1215 cm^{-1} (C−O stretching in epoxy), and 1032 cm^{-1} (C−O stretching in alkoxy), respectively. The intensity of peaks at 1725 and 1032 cm^{-1} is decreased on amine functionalization due to the formation of −CONH linking between GO and EDTA. After EDTA functionalization, a new strong peak appears at 1200 cm^{-1} due to the stretching vibration of C−O in COO^- of EDTA. A strong peak at 1540 cm^{-1} is due to the asymmetric and symmetric vibrations of COO^- from EDTA. Another new peak at 1018 cm^{-1} is due to the N−C bonds present in EDTA. From the FTIR spectra, it is observed that all of the oxygen

https://doi.org/10.1021/acsomega.2c06080
ACS Omega 2022, 7, 45469−45480

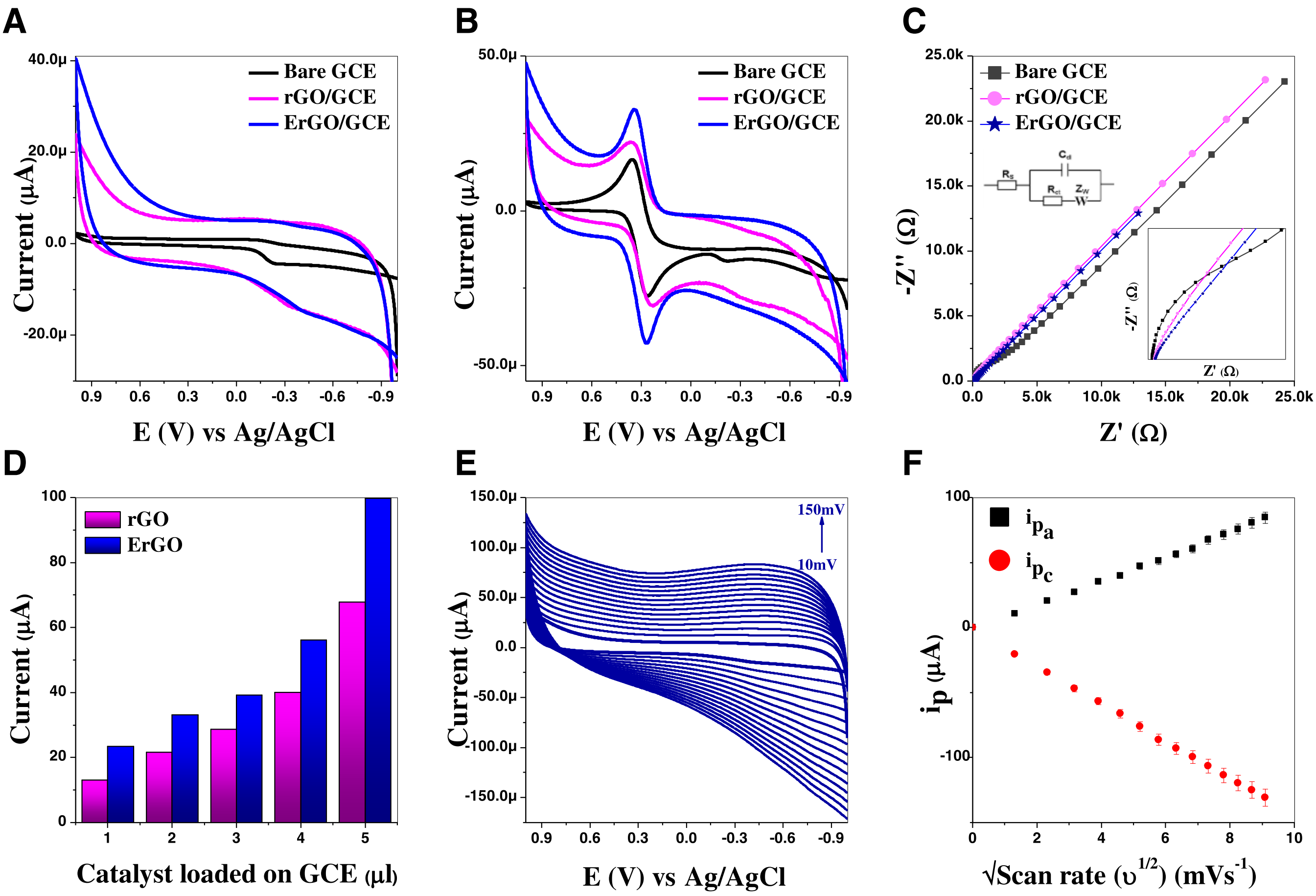

Figure 3. Cyclic voltammograms of GCE vs rGO/GCE vs ErGO/GCE in (A) acetate buffer and the (B) $[Fe(CN)_6]^{3-/4-}$/KCl system at a scan rate of 10 mV/s. (C) Nyquist plots recorded in 5 mM $[Fe(CN)_6]^{3-/4-}$/KCl. (D) Bar graph for the loading effect of the electrocatalyst material on GCE in sodium acetate buffer. (E) Effect of the scan rate recorded using ErGO/GCE in acetate buffer. (F) Calibration plot showing the linear relationship of current with the square root of scan rate.

functional groups are dramatically reduced in rGO, while in ErGO, the characteristic peaks of EDTA are retained and only the oxygen functional groups on the GO surface are reduced.

The thermogravimetric analysis (TGA) of the GO and ErGO samples was performed to determine the structural changes before and after functionalization (Figure 1C). The samples were heated from 100 to 1200 °C at a heating rate of 20 °C per min. The initial decomposition in the range of 30−100 °C is due to the evaporation of H_2O molecules. In the case of GO, the weight loss between 150 and 300 °C is due to the loss of oxygen functionalities and the final weight loss between 300 and 1200 °C is due to the decomposition of graphene layers. In the case of ErGO, the decomposition was observed in the range of 250−700 °C due to the loss of EDTA groups. For the ErGO sample, the weight loss is initiated at a higher temperature, comparatively, which reveals the stability of the material.

The ζ potential values obtained from dynamic light scattering (DLS) analysis further suggest that ErGO is more stable than GO and rGO (Figure 1D). The sample (1.0 mg) was dissolved in 10 mL of double-distilled water for the DLS analysis. The ζ potential values obtained are −23.2, −46.3, and −58.0 mV for GO, rGO, and ErGO, respectively. High negative values of ζ potential suggest their high stability in aqueous dispersion or negligible sedimentation tendency.

The band gap values for rGO and ErGO were evaluated to be 2.99 and 2.49 eV, respectively, using the Kubelka−Munk equation from the UV-DRS spectrum (Figure 1E,F). The decrease in band gap energy value can be due to increasing surface concentration upon functionalization. Also, the absorption band in the visible region is shifted due to changes in lattice parameters and band gap transition (inset, Figure 1E,F). This shows the high conductivity behavior of the ErGO electrocatalyst compared to rGO.

Morphological changes of GO due to functionalization and reduction were investigated by SEM and FESEM analysis (Figure 2). Based on the results of EDAX attached to SEM, Figure 2A shows the GO layers with the presence of oxygen functionalities; Figure 2B reveals the image of rGO where all of the oxygen-containing functional groups are reduced, while Figure 2C represents the presence of EDTA groups on the reduced graphene surface. Figure 2D−F show layered patterns of GO, rGO, and ErGO in the FESEM images. From the FESEM-EDAX images, EDTA groups may be present on the edges (Figure 2F). The elemental (wt %) analysis values from EDAX spectra attached to FESEM reveal oxygen-rich GO (Figure 2G), decreased oxygen content after reduction (Figure 2H) and high nitrogen content in ErGO from EDTA (Figure 2I). All results are from the previously reported literature.[37]

3.2. Electrochemical Behavior of the Modified Electrodes.

Preliminary electrochemical characterizations of

https://doi.org/10.1021/acsomega.2c06080
ACS Omega 2022, 7, 45469−45480

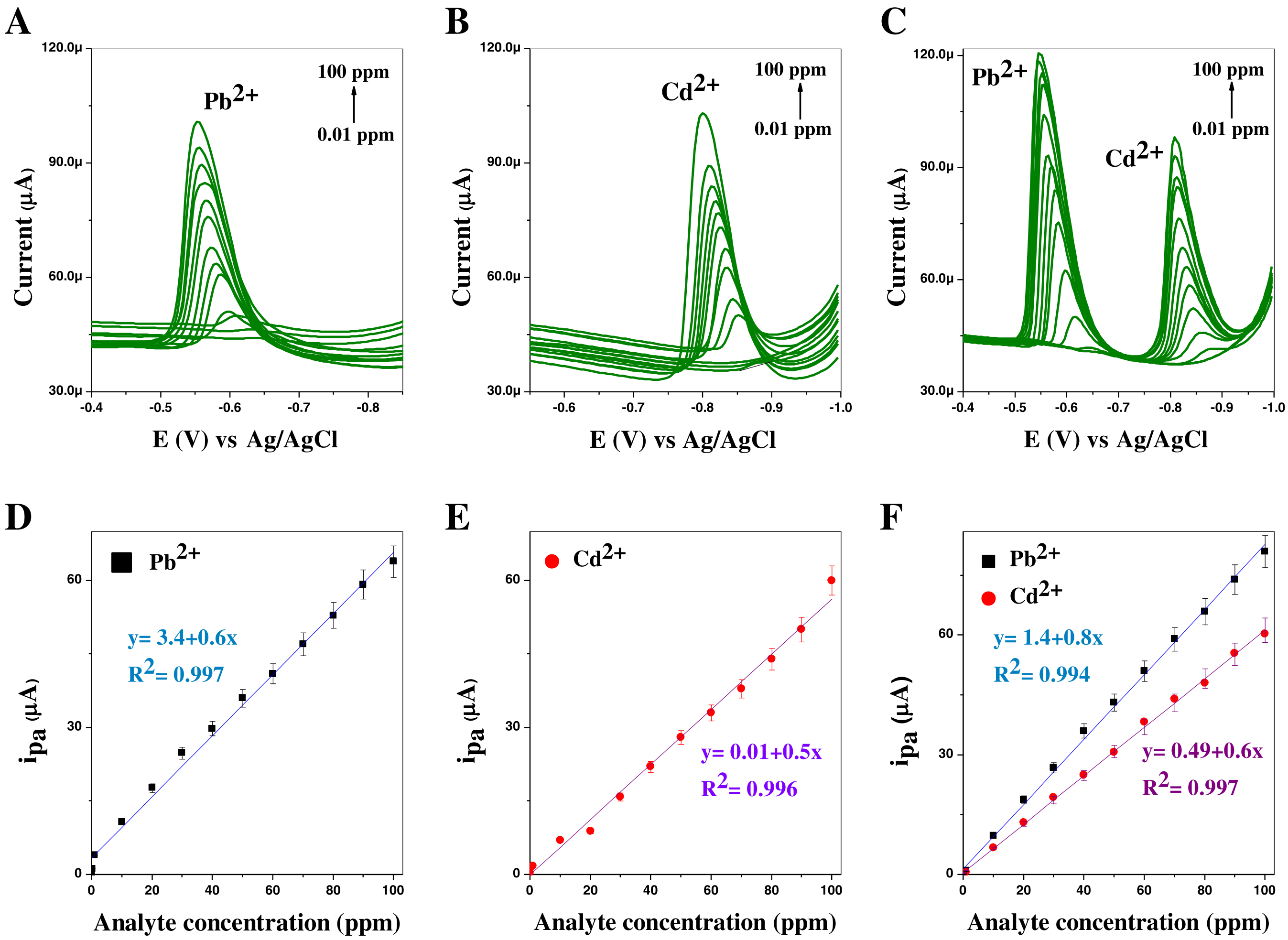

Figure 4. DPV graphs of individual detection of (A) Pb^{2+} and (B) Cd^{2+}. (C) Simultaneous detection of Pb^{2+} and Cd^{2+} on ErGO/GCE and (D−F) their respective calibration curves of various concentrations (0.01−100 ppm) in 0.1 M sodium acetate buffer (pH 5).

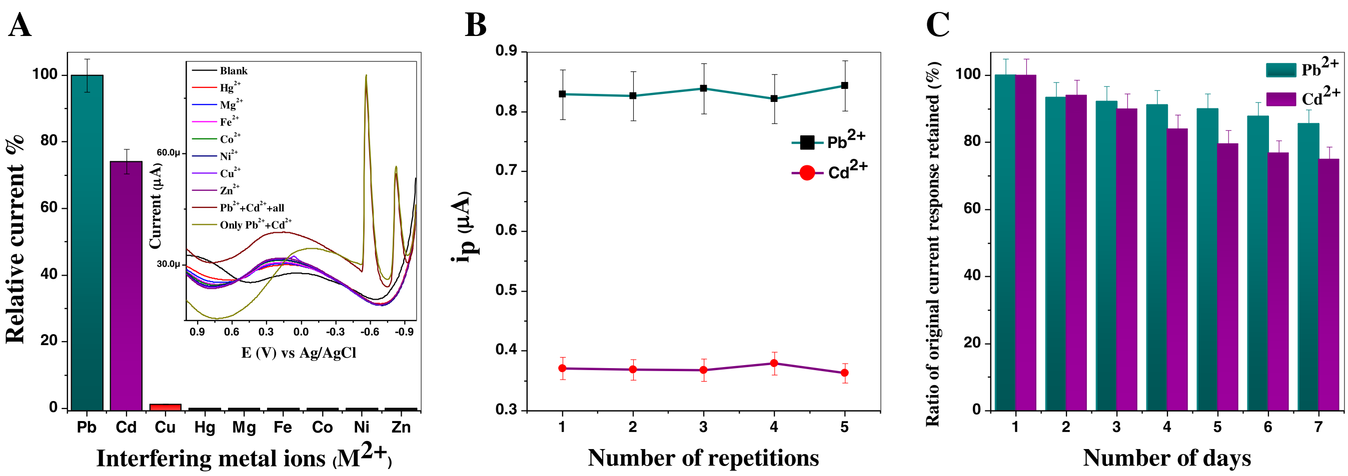

Figure 5. (A) Selectivity of Pb^{2+} and Cd^{2+} ions on ErGO/GCE among other possible interfering ions in acetate buffer (inset: DPV of all individual metal ions, simultaneous Pb^{2+} and Cd^{2+} ions in the presence and absence of other metal ions). (B) Repeatability of simultaneous analysis on ErGO/GCE for 5 repetitions. (C) Stability of ErGO/GCE for simultaneous analysis for 7 days.

rGO and ErGO were evaluated by CV and EIS.[41] The cyclic voltammograms were recorded for rGO-modified GCE and ErGO-modified GCE between the potential windows of 1 and −1 V vs Ag/AgCl at a scan rate of 10 mV/s in different electrolytic media having a 0.1 M concentration. The electrode performance was found to be better in 0.1 M sodium acetate buffer (pH 5) (Figure S1).

The non-Faradaic, band-like current response in sodium acetate buffer evidences the conductive nature of the material. The obtained current value for ErGO/GCE (curve blue) was 20 times higher compared to rGO/GCE (curve pink) (Figure

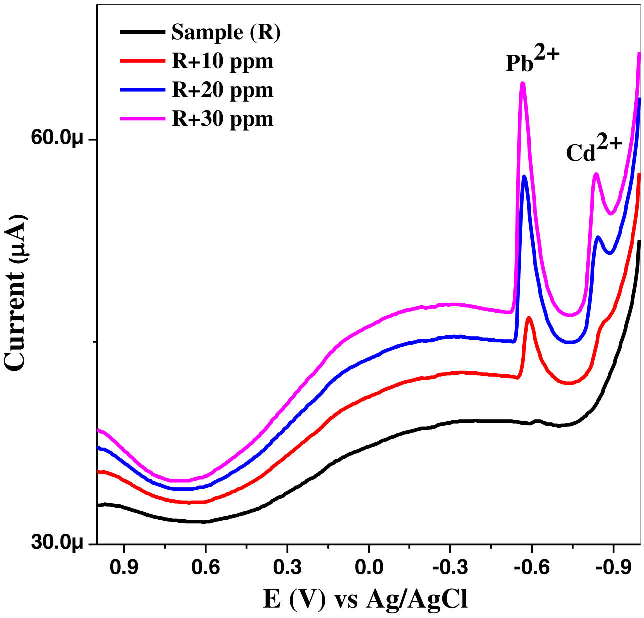

Figure 6. DPV responses of the ErGO/GCE toward bCd^{2+} and Pb^{2+} ions in the real sample between potential window 1 and −1 V under previously optimized conditions.

Table 1. Quantitation of Cd^{2+} and Pb^{2+} Ions in Water Samples on the ErGO/GCE

real sample	metal ions	added (ppm)	found (ppm)	recovery (%)
river water	Cd^{2+}	0	0	
		10	10.2	102 ± 0.01
		20	20.22	101.1 ± 0.02
		30	30.3	101 ± 0.08
	Pb^{2+}	0	0.2	
		10	9.6	96 ± 0.04
		20	19.3	96.5 ± 0.16
		30	30.3	101 ± 0.14

3A). The stability of the material on the GCE was attained through continuous CV responses, showing no decrement in the current (Figure S2).

The electron transfer nature of the modified electrode was evaluated with the help of the $[Fe(CN_6)]^{3-/4-}$ redox mediator (Figure 3B). The redox peak increased with an increased peak-to-peak potential separation value, which shows the high conductivity of rGO/GCE (curve pink), whereas, the faradaic peak current was further enhanced while the peak-to-peak separation decreased for ErGO/GCE (curve blue). The cyclic voltammogram shows a decreased overpotential and an increase in the current factor by 1.2 times for ErGO/GCE compared to rGO/GCE (Figure 3B). The Ep values are substituted in the formula $\Delta E_p = (E_{pa} - E_{pc})$ and obtained as 88, 130, and 76 mV for bare GCE, rGO/GCE, and ErGO/GCE, respectively. From the Randles−Sevcik equation, the electroactive surface area (A_{geo} in cm^2) is calculated by substituting the constant values of the diffusion coefficient (D in $cm^2 s^{-1}$), the number of electrons (n), scan rate (ν in V/s), and concentration (C in mol cm^{-3}). The surface areas are calculated to be 0.071, 0.058, and 0.089 cm^2 for GCE, rGO/GCE, and ErGO/GCE, proving the excellent electrocatalytic activity of the ErGO/GCE.

Electrochemical impedance spectroscopy (EIS) measurements were carried out to further investigate the electrochemical properties and stability of the electrocatalyst materials in the 5 mM $[Fe(CN)_6]^{3-/4-}$/KCl system in a frequency range of 10^5 to 0.1 Hz. The Z″ is the imaginary component of the impedance and Z' is the real component of impedance in the Nyquist plot. The shorter linear region and smaller semicircle diameter reveal lower interfacial charge-transfer resistance with superior electrochemical properties,[42,43] as well as the minimum influence of Warburg impedance on the efficiency of ErGO/GCE (curve blue) compared to bare GCE (curve black) and rGO/GCE (curve pink)[44] (Figure 3C). The diameter of the semicircle demonstrates the interfacial charge-transfer resistance. From the inset of Figure 3C, a large diameter semicircle was seen for the bare GCE with a larger R_{ct} value of 1.63 kΩ, while the rGO/GCE and ErGO/GCE showed negligible R_{ct} values of 5.14 and 1.18 $\mu\Omega$, respectively, after fitting the experimental data with Randles equivalence circuit model. This suggests the fast ion diffusion in electrolytes and adsorption on the electrodes resulting in higher charge-transfer between adsorbed metal ions and electrocatalysts with high efficiency (Scheme 1).

The loading effect of electrocatalyst materials was optimized in sodium acetate buffer using cyclic voltammetry and compared as a bar chart to understand the physical nature and stability of the modified electrode (Figure 3D). From the prepared dispersion, a range of 1−5 μL of catalyst dispersion was coated on the surface of the GCE. The Faradaic current increased in proportion to the catalyst loaded on GCE, revealing the active sites present on the catalyst. The current response for ErGO is better compared to rGO, which shows the efficiency of the material after functionalization. An optimum volume of 3 μL of the rGO and ErGO dispersion was loaded on the GCE for further electrochemical studies to enable a neat and efficient drop-casting and to avoid overflowing of the catalyst on a 3 mm GCE surface.

The effect of scan rates ranging from 10 to 100 mV/s was performed for ErGO/GCE in an acetate buffer solution (Figure 3E). The conductance band-like response increased to the square root of the scan rate (Figure 3F). No electron transfer behavior was seen in the catalyst; however, it confirms the conductive nature of ErGO, which improves the sensitivity as a catalyst material. The obtained results suggest that ErGO/GCE showed better performance compared to rGO/GCE and bare GCEs.

3.3. Electrochemical Detection by Differential Pulse Voltammetry. The simultaneous DPV curves of Pb^{2+} and Cd^{2+} ions on bare GCE, rGO/GCE, and ErGO/GCE were recorded to compare the current responses. The highest response was observed for ErGO/GCE due to low charge-transfer resistance and high conductivity (Figure S3). A minimal or negligible current response for Pb^{2+} and Cd^{2+} ions was seen on bare GCE, while the i_p values slightly increased on rGO/GCE and large i_p values were seen on the ErGO/GCE (Table S1).

The pH effect of acetate buffer was studied on the ErGO/GCE. The results revealed that the ErGO-modified electrode attained maximum peak current for both the Pb^{2+} and Cd^{2+} ions between solution pH of 4 and 5. The actual pH of the sodium acetate buffer prepared was 5. Hence, pH changes for the buffer solution were avoided before analysis (Figure S4).

The electrochemical quantitation of Pb^{2+} and Cd^{2+} ions was carried out individually (Figures 4A,B) and simultaneously (Figure 4C) with ErGO-modified GCE for concentrations ranging from 0.01 to 100 ppm in sodium acetate buffer. The

https://doi.org/10.1021/acsomega.2c06080
ACS Omega 2022, 7, 45469−45480

Table 2. Comparison of LODs and Sensitivity for Pb^{2+} and Cd^{2+} Ions Reported in the Literature

electrode substrate	preparation method	real sample	technique	analytes detected	sensitivity	LOD	ref
SnO_2/rGO/GCE	wet chemical method	drinking water	SWASV	Cd^{2+}	18.4 μA/μM	0.10 nM/L (0.037 ppb)	46
				Pb^{2+}	18.6 μAμM	0.18 nM/L (0.011 ppb)	
rGO/$NiWO_4$/C paper	hydrothermal method	milk and fruit juices	DPASV	Cd^{2+}	0.8 μA/μM	0.11 nM/L (0.012 ppb)	47
				Pb^{2+}	14.7 μA/μM	0.20 nM/L (0.041 ppb)	
NCQDs-GO/GCE	microwave-assisted method	tap water and lake water	ASV	Cd^{2+}		7.45 μg/L (7.45 ppb)	48
				Pb^{2+}		1.17 μg/L (1.17 ppb)	
rGO/CNT/Bi composite electrode	solvothermal method	water samples	SWASV	Cd^{2+}	262 nA/ppb	0.6 ppb	49
				Pb^{2+}	926 nA/ppb	0.2 ppb	
ZnO/graphene/SPCE	thermal decomposition method	wastewater	SWASV	Cd^{2+}	0.2941 μA/μg	0.6 μg/L (0.6 ppb)	50
				Pb^{2+}	0.2803 μA/μg	0.8 μg/L (0.8 ppb)	
graphene/gold nanoparticles/modified L-cysteine/GCE	chemical reflux method	various water samples	SWASV	Cd^{2+}	2.2 μA/nM	0.06 nM/L (0.007 ppb)	51
				Pb^{2+}	3.2 μA/nM	0.04 nM/L (0.008 ppb)	
rGO/Sb/GCE	chemical reduction	chamomile tea	SWASV	Cd^{2+}	3.06 μA/μM	70.03 nM/L (8.218 ppb)	52
				Pb^{2+}	21.3 μA/μM	45.50 nM/L (9.427 ppb)	
Bi/LC-rGO/DSPE	electrochemical reduction	decorative materials	LSV/DPV	Cd^{2+}	065 μA/μg	0.1 μg/L (0.1 ppb)	53
				Pb^{2+}	0.50 μA/μg	0.08 μg/L (0.08 ppb)	
Co_3O_4/GO	solvothermal	real water	DPASV	Cd^{2+}	1.15 μA/μM	57 nM/L (6.69 ppb)	54
				Pb^{2+}	4 μA/μM	29.4 nM/L (6.09 ppb)	
$ZnFe_2O_4$/rGO/GCE	solvothermal	industrial effluent	DPASV	Cd^{2+}		0.71 ppb	55
				Pb^{2+}		0.89 ppb	
graphdiyne/GCE	chemical method	lake water	SWASV	Cd^{2+}		0.46 nM/L (0.054 ppb)	56
				Pb^{2+}		1.72 nM/L (0.356 ppb)	
nZVI/porous C/GCE	biomass reduction	drinking water	SWSV	Cd^{2+}	0.2336 μA/μg	0.1926 μg/L (0.1926 ppb)	57
				Pb^{2+}	0.2160 μA/μg	0.2082 μg/L (0.2082 ppb)	
Fe_2O_3/Bi_2O_3/GCE	ultrasonication	milk and water sample	SWASV	Cd^{2+}		0.56 nM (0.063 ppb)	58
				Pb^{2+}		0.36 nM (0.075 ppb)	
Bi_2O_3/MnO_2/GO/GCE	ultrasonication	water sample	SWASV	Pb^{2+}	53.43 μA/μM	2 nM (0.41 ppb)	59
ErGO/GCE	chemical functionalization & green reduction method	river water	DPV	Cd^{2+}	0.8138 μA/ppm	1.02 ppb	this work
				Pb^{2+}	0.6082 μA/ppm	2.52 pb	

https://doi.org/10.1021/acsomega.2c06080
ACS Omega 2022, 7, 45469−45480

peak current appeared at potentials of −0.6 and −0.85 V for Pb^{2+} and Cd^{2+} ions, respectively. The peak current increased with the addition of Pb^{2+} and Cd^{2+} concentration.

Both individual and simultaneous voltammograms of Pb^{2+} and Cd^{2+} ions showed a linear relationship between the analyte concentrations and peak current ranging from 0.01 to 100 ppm (Figure 4D−F). For individual analysis, the sensitivity and regression coefficient (R^2) values were found to be 0.6 μA/ppm and 0.997 for Pb^{2+} ions and 0.50 μA/ppm and 0.996 for Cd^{2+} ions, whereas 0.8 μA/ppm and 0.994 for Pb^{2+} ions and 0.6 μA/ppm and 0.997 for Cd^{2+} ions in the case of simultaneous analysis. The results were almost similar for individual and simultaneous analysis, thereby showing no mutual interferences between Pb^{2+} and Cd^{2+} ions during simultaneous analysis.

The standard deviation (σ) value was obtained from ten blank measurements of 0.1 M sodium acetate buffer electrolyte. The slope (m) value was obtained from the calibration plot of the analyte concentration.[45] The LOD ($3\sigma/m$) and LOQ ($10\sigma/m$) values were calculated to be 1.02 and 3.41 ppb for Pb^{2+} ions and 2.52 ppb and 8.40 ppb for Cd^{2+} ions from the calibration curves of simultaneous analysis.

3.4. Selectivity, Repeatability, and Stability. Possible interfering metal ions such as Hg^{2+}, Mg^{2+}, Fe^{2+}, Co^{2+}, Ni^{2+}, Cu^{2+}, and Zn^{2+} ions (100 ppm) were analyzed individually and along with the target analyzed mixture. The presence of other metal ions did not influence the peak current and peak potential of Pb^{2+} and Cd^{2+} ions (Figure 5A). A negligible peak current was observed for Cu^{2+} and Hg^{2+} ions, whereas no peak signals were seen for other ions. Also, no shift in the peak potential and peak current were observed for target analytes. The selectivity of the electrocatalyst material toward Pb^{2+} and Cd^{2+} ions is due to the chelation of EDTA (Scheme 1) and pH of the electrolyte (inset of Figure 5A).

The repeatability of the ErGO/GCE was determined by performing five repetitive measurements of simultaneous DPV responses for 1 ppm of Pb^{2+} and Cd^{2+} in 0.1 M sodium acetate buffer electrolyte (pH 5). The current intensities were almost similar with relative standard deviation (RSD, n = 5) values of 1.00% for Pb^{2+} and 1.64% for Cd^{2+} using the ErGO/GCE (Figure 5B).

Stability was evaluated by time-dependent DPV responses. The ErGO-modified GCE, stored at room temperature retained a current response of 85.5% of Pb^{2+} and 75% of Cd^{2+}, exhibiting good stability for 7 days (Figure 5C).

3.5. Analysis of the Real Water Sample. To validate the practical application of the ErGO/GCE toward electrochemical quantitation of Pb^{2+} and Cd^{2+} ions, the collected river water sample was subjected to DPV analysis. DPV was recorded in the river water sample without spiking first and with known concentrations of 10, 20, and 30 ppm analytes, which are represented as R + 10, R + 20, and R + 30 ppm by the standard addition method (Figure 6). The concentrations of Pb^{2+} and Cd^{2+} ions in the river water sample were found as represented in Table 1. The peak response for Cd^{2+} ions was not observed distinctly in the real sample originally; however, on standard addition, the peak signals corresponding to Cd^{2+} ions were observed. These results demonstrate satisfactory recovery values of the target analytes (96−101% for Pb^{2+} ions and 101−102% for Cd^{2+} ions). The river water contained only 200.2 ± 0.38 ppb of Pb^{2+} ions (mean ± stdev, n = 3), determined by the DPV technique. The result was compared with the ICP-OES analysis results and the concentration of Pb^{2+} ions was 199.90 ± 0.49 (mean ± stdev, n = 3), which is highly comparable to DPV analysis results. Hence, the developed sensor can be successfully used for the quantitation of Pb^{2+} and Cd^{2+} ions in environmental water samples.

Table 2 summarizes and compares the LOD values of the ErGO/GCE from the reported works in the literature. The data are a review of GCE modified with GO-based materials for the simultaneous voltammetric detection of Cd^{2+} and Pb^{2+} ions in various samples such as milk, tea, wastewater, etc. Though there are works in the literature that report trace-level detection limits for Pb^{2+} and Cd^{2+} ions, the present work meets the acceptable LOD, LOQ, and sensitivity values using the DPV technique. The present work highlights the significance of functionalized rGO-based materials in the field of electrochemical detection and quantitation. The electrode modification and voltammetric quantitation methods presented in this paper are simple, low-cost, and fast. Therefore, Table 2 presents the reliability of the present work on par with the reported works in the literature for their practical applications on environmental samples.[46−59]

4. CONCLUSIONS

In summary, an ErGO/GCE-modified electrode was successfully developed for the simultaneous quantitation of Cd^{2+} and Pb^{2+} ions in environmental samples. ErGO was synthesized by chemical functionalization followed by green reduction methods. The changes in the material after functionalization and reduction were studied by various physiochemical characterization techniques such as XRD, FTIR, TGA, DLS, and UV-DRS. The electrochemical behavior of the modified electrode was analyzed by CV and EIS. The GCE was modified with ErGO dispersion by a simple drop-casting method and applied for the simultaneous quantitation of Cd^{2+} and Pb^{2+} ions by the DPV technique. The developed electrode substrate showed a satisfactory linear range, high sensitivity and selectivity, good repeatability, stability, negligible interference of other metal ions, and an acceptable low detection limit, below the standard values set by the WHO. In addition, the synthesized electrocatalyst was explored for its practical applications in the river water sample and the results were compared with ICP-OES results. Therefore, the developed electrocatalyst material could be employed for simultaneous monitoring and assessment of heavy-metal-ion load in real environmental samples.

■ ASSOCIATED CONTENT

Supporting Information

The Supporting Information is available free of charge at https://pubs.acs.org/doi/10.1021/acsomega.2c06080.

CV graphs of the ErGO/GCE in different 0.1 M electrolytes (potassium chloride, phosphate, acetate, and sulfuric acid) to study their effects on the current factor; current stability of ErGO/GCE for repeated 50 CV cycles at a scan rate of 10 mV/s in acetate buffer within the potential window from 1 to −1 V; DPV graphs of bare GCE, rGO/GCE, and ErGO/GCE in sodium acetate buffer electrolyte (0.1 M) containing 1 ppm of Pb^{2+} and Cd^{2+} each with previously optimized conditions; DPV graph of ErGO/GCE in acetate buffer of different pH values showing better current response for simultaneous analysis of Pb^{2+} and Cd^{2+} at pH 4 and pH 5 (actual buffer pH = 5); comparison of current

https://doi.org/10.1021/acsomega.2c06080
ACS Omega 2022, 7, 45469−45480

values of bare GCE, rGO/GCE, and ErGO/GCE for simultaneous quantitation of Pb^{2+} and Cd^{2+} ions (PDF)

AUTHOR INFORMATION

Corresponding Author

Badal Kumar Mandal − *Trace Elements Speciation Research Laboratory, Department of Chemistry, School of Advanced Sciences, Vellore Institute of Technology, Vellore 632014 Tamil Nadu, India;* orcid.org/0000-0003-2419-5247; Email: badalmandal@vit.ac.in

Author

Nishanthi Vasanthi Sridharan − *Trace Elements Speciation Research Laboratory, Department of Chemistry, School of Advanced Sciences, Vellore Institute of Technology, Vellore 632014 Tamil Nadu, India;* orcid.org/0000-0003-4729-8492

Complete contact information is available at: https://pubs.acs.org/10.1021/acsomega.2c06080

Notes

The authors declare no competing financial interest.

ACKNOWLEDGMENTS

The authors thank the Vellore Institute of Technology, Vellore 632014, India for the financial support, working platform, and sophisticated instrumental facilities (SIF-VIT) provided to complete the study. Also, the authors deeply acknowledge the help of Mr. Srinivas S. (VIT, Vellore) during the handling of electrochemical workstations, Dr. Senthil Kumar Annamalai (VIT, Vellore) for the EIS study, and Dr. Bhaskar Das (VIT, Vellore) for ICP-OES analysis of this research work. In addition, the authors acknowledge the help of Dr. Mohan Kumar K (Instituto de Ciencias Físicas, Universidad Nacional Autónoma de México) and Dr. Naveen Kumar Reddy Bogireddy (Consorcio Universidad Nacional Autonoma de Mexico) for the characterization of the synthesized electrocatalysts.

REFERENCES

(1) Wu, X.; Cobbina, S. J.; Mao, G.; Xu, H.; Zhang, Z.; Yang, L. A review of toxicity and mechanisms of individual and mixtures of heavy metals in the environment. *Environ. Sci. Pollut. Res. Int.* **2016**, *23*, 8244−8259.

(2) Balali-Mood, M.; Naseri, K.; Tahergorabi, Z.; Khazdair, M. R.; Sadeghi, M. Toxic Mechanisms of Five Heavy Metals: Mercury, Lead, Chromium, Cadmium, and Arsenic. *Front. Pharmacol.* **2021**, *12*, No. 643972.

(3) Zhou, F.; Yin, G.; Gao, Y.; Liu, D.; Xie, J.; Ouyang, L.; Fan, Y.; Yu, H.; Zha, Z.; Wang, K.; Shao, L.; Feng, C.; Fan, G. Toxicity assessment due to prenatal and lactational exposure to lead, cadmium and mercury mixtures. *Environ. Int.* **2019**, *133*, No. 105192.

(4) Rahman, Z.; Singh, V. P. The relative impact of toxic heavy metals (THMs) (arsenic (As), cadmium (Cd), chromium (Cr)(VI), mercury (Hg), and lead (Pb)) on the total environment: an overview. *Environ. Monit. Assess.* **2019**, *191*, No. 419.

(5) Rehman, A. U.; Fayaz, M.; Lv, H.; Liu, Y.; Zhang, Y.; Wang, Y.; Du, L.; Wang, R.; Shi, K. Controllable Synthesis of a Porous PEI-Functionalized Co_3O_4/rGO Nanocomposite as an Electrochemical Sensor for Simultaneous as Well as Individual Detection of Heavy Metal Ions. *ACS Omega* **2022**, *7*, 5870−5882.

(6) Lu, Y.; Liang, X.; Niyungeko, C.; Zhou, J.; Xu, J.; Tian, G. A review of the identification and detection of heavy metal ions in the environment by voltammetry. *Talanta* **2018**, *178*, 324−338.

(7) Deshmukh, M. A.; Patil, H. K.; Bodkhe, G. A.; Yasuzawa, M.; Koinkar, P.; Ramanaviciene, A.; Shirsat, M. D.; Ramanavicius, A. EDTA-modified PANI/SWNTs nanocomposite for differential pulse voltammetry based determination of Cu(II) ions. *Sens. Actuators, B* **2018**, *260*, 331−338.

(8) Chang, J.; Zhou, G.; Christensen, E. R.; Heideman, R.; Chen, J. Graphene-based sensors for detection of heavy metals in water: A review Chemosensors and Chemoreception. *Anal. Bioanal. Chem.* **2014**, *406*, 3957−3975.

(9) Li, Q.; Xia, Y.; Wan, X.; Yang, S.; Cai, Z.; Ye, Y.; Li, G. Morphology-dependent MnO2/nitrogen-doped graphene nanocomposites for simultaneous detection of trace dopamine and uric acid. *Mater. Sci. Eng. C* **2020**, *109*, No. 110615.

(10) Li, G.; Qi, X.; Wu, J.; Xu, L.; Wan, X.; Liu, Y.; Chen, Y.; Li, Q. Ultrasensitive, label-free voltammetric determination of norfloxacin based on molecularly imprinted polymers and Au nanoparticle-functionalized black phosphorus nanosheet nanocomposite. *J. Hazard. Mater.* **2022**, *436*, No. 129107.

(11) Smith, A. T.; LaChance, A. M.; Zeng, S.; Liu, B.; Sun, L. Synthesis, properties, and applications of graphene oxide/reduced graphene oxide and their nanocomposites. *Nano Mater. Sci.* **2019**, *1*, 31−47.

(12) Rowley-Neale, S. J.; Randviir, E. P.; Abo Dena, A. S.; Banks, C. E. An overview of recent applications of reduced graphene oxide as a basis of electroanalytical sensing platforms. *Appl. Mater. Today* **2018**, *10*, 218−226.

(13) Kornilov, D. Y.; Gubin, S. P. Graphene Oxide: Structure, Properties, Synthesis, and Reduction (A Review). *Russ. J. Inorg. Chem.* **2020**, *65*, 1965−1976.

(14) Eshlaghi, M. A.; Kowsari, E.; Ehsani, A.; Akbari-Adergani, B.; Hekmati, M. Functionalized graphene oxide GO-[imi-$(CH_2)_2$-NH_2] as a high efficient material for electrochemical sensing of lead: Synthesis surface and electrochemical characterization. *J. Electroanal. Chem.* **2020**, *858*, No. 113784.

(15) Li, Q.; Wu, J.; Liu, Y.; Qi, X.; Jin, H.; Yang, C.; Liu, J.; Li, G.; He, Q. Recent advances in black phosphorus-based electrochemical sensors: A review. *Anal. Chim. Acta* **2021**, *1170*, No. 338480.

(16) Li, G.; Wu, J.; Qi, X.; Wan, X.; Liu, Y.; Chen, Y.; Xu, L. Molecularly imprinted polypyrrole film-coated poly(3,4-ethylene dioxythiophene): polystyrene sulfonate-functionalized black phosphorene for the selective and robust detection of norfloxacin. *Mater. Today Chem.* **2022**, No. 101043.

(17) Hou, S.; Kasner, M. L.; Su, S.; Patel, K.; Cuellari, R. Highly sensitive and selective dopamine biosensor fabricated with silanized graphene. *J. Phys. Chem. C* **2010**, *114*, 14915−14921.

(18) Yakout, A. A.; Albishri, H. M. Solvothermal synthesis of EDTA-functionalized magnetite-carboxylated graphene oxide nanocomposite as a potential magnetic solid phase extractor of p-phenylenediamine from environmental samples. *J. Dispersion Sci. Technol.* **2019**, *40*, 369−377.

(19) Zuo, Y.; Han, Y.; Zhang, G.; Fan, L.; Liu, Z.; Guo, Y. EDTA-β-cyclodextrin functionalized graphene for electrochemical detection and scavenge of DPPH radical. *J. Appl. Electrochem.* **2021**, *51*, 1731−1739.

(20) Madadrang, C. J.; Kim, H. Y.; Gao, G.; Wang, N.; Zhu, J.; Feng, H.; Gorring, M.; Kasner, M. L.; Hou, S. Adsorption behavior of EDTA-graphene oxide for Pb (II) removal. *ACS Appl. Mater. Interfaces* **2012**, *4*, 1186−1193.

(21) Cui, L.; Wang, Y.; Gao, L.; Hu, L.; Yan, L.; Wei, Q.; Du, B. EDTA functionalized magnetic graphene oxide for removal of Pb(II), Hg(II) and Cu(II) in water treatment: Adsorption mechanism and separation property. *Chem. Eng. J.* **2015**, *281*, 1−10.

(22) Shahzad, A.; Miran, W.; Rasool, K.; Nawaz, M.; Jang, J.; Lim, S.; Lee, D. S. Heavy metals removal by EDTA-functionalized chitosan graphene oxide nanocomposites. *RSC Adv.* **2017**, *7*, 9764−9771.

(23) Jiang, Y.; Liu, C.; Huang, A. EDTA-Functionalized Covalent Organic Framework for the Removal of Heavy-Metal Ions. *ACS Appl. Mater. Interfaces* **2019**, *11*, 32186−32191.

(24) Wang, H.; Lai, X.; Zhao, W.; Chen, Y.; Yang, X.; Meng, X.; Li, Y. Efficient removal of crystal violet dye using EDTA/graphene oxide functionalized corncob: A novel low cost adsorbent. *RSC Adv.* **2019**, *9*, 21996−22003.
(25) Khadivi, S. M.; Edjlali, L.; Akbarzadeh, A.; Seyyedi, K. Enhanced adsorption behavior of amended EDTA−graphene oxide for methylene blue and heavy metal ions. *Int. J. Environ. Sci. Technol.* **2019**, *16*, 8151−8160.
(26) Keyvani, F.; Rahpeima, S.; Javanbakht, V. Synthesis of EDTA-modified magnetic activated carbon nanocomposite for removal of permanganate from aqueous solutions. *Solid State Sci.* **2018**, *83*, 31−42.
(27) Verma, M.; Kumar, A.; Lee, I.; Kumar, V.; Park, J.; Kim, H. Simultaneous capturing of mixed contaminants from wastewater using novel one-pot chitosan functionalized with EDTA and graphene oxide adsorbent. *Environ. Pollut.* **2022**, *304*, No. 119130.
(28) Teng, Z.; Lv, H.; Wang, L.; Liu, L.; Wang, C.; Wang, G. Voltammetric Sensor Modified by EDTA-immobilized Graphene-like Carbon Nitride Nanosheets: Preparation, Characterization and Selective Determination of Ultra-Trace Pb (II) in Water Samples. *Electrochim. Acta* **2016**, *212*, 722−733.
(29) Moutcine, A.; Chtaini, A. Electrochemical determination of trace mercury in water sample using EDTA-CPE modified electrode. *Sens. Bio-Sens. Res.* **2018**, *17*, 30−35.
(30) Yi, W.; He, Z.; Fei, J.; He, X. Sensitive electrochemical sensor based on poly(l-glutamic acid)/graphene oxide composite material for simultaneous detection of heavy metal ions. *RSC Adv.* **2019**, *9*, 17325−17334.
(31) Ercarikci, E.; Alanyalioglu, M. Dual-Functional Graphene-Based Flexible Material for Membrane Filtration and Electrochemical Sensing of Heavy Metal Ions. *IEEE Sens. J.* **2021**, *21*, 2468−2475.
(32) Mahadik, M.; Patil, H.; Bodkhe, G.; Ingle, N.; Sayyad, P.; Al-Gahhouri, T.; Shirsat, S. M.; Shirsat, M. EDTA Modified PANI/GO Composite Based Detection of Hg (II) Ions. *Front. Mater.* **2020**, *7*, No. 81.
(33) Toghan, A.; Abd-Elsabour, M.; Abo-Bakr, A. M. A novel electrochemical sensor based on EDTA-NQS/GC for simultaneous determination of heavy metals. *Sens. Actuators, A* **2021**, *322*, No. 112603.
(34) Banavath, R.; Srivastava, R.; Bhargava, P. EDTA derived graphene supported porous cobalt hexacyanoferrate nanospheres as a highly electroactive nanocomposite for hydrogen peroxide sensing. *Catal. Sci. Technol.* **2022**, *12*, 2369−2383.
(35) Hummers, W. S.; Offeman, R. E. Preparation of Graphitic Oxide. *J. Am. Chem. Soc.* **1958**, *80*, No. 1339.
(36) Perera, S. D.; Mariano, R. G.; Nijem, N.; Chabal, Y.; Ferraris, J. P.; Balkus, K. J. Alkaline deoxygenated graphene oxide for supercapacitor applications: An effective green alternative for chemically reduced graphene. *J. Power Sources* **2012**, *215*, 1−10.
(37) Mahmoudian, M.; Nozad, E.; Hosseinzadeh, M. Characterization of EDTA functionalized graphene oxide/polyethersulfone (FGO/PES) nanocomposite membrane and using for elimination of heavy metal and dye contaminations. *Polymer* **2018**, *42*, 434−445.
(38) Maddinedi, S. B.; Mandal, B. K.; Fazlur-Rahman, N. K. High reduction of 4-nitrophenol using reduced graphene oxide/Ag synthesized with tyrosine. *Environ. Chem. Lett.* **2017**, *15*, 467−474.
(39) Si, Y.; Liu, J.; Chen, Y.; Miao, X.; Ye, F.; Liu, Z.; Li, J. rGO/AuNPs/tetraphenylporphyrin nanoconjugate-based electrochemical sensor for highly sensitive detection of cadmium ions. *Anal. Methods* **2018**, *10*, 3631−3636.
(40) Yang, S.; Liu, P.; Wang, Y.; Guo, Z.; Tan, R.; Qu, L. Electrochemical sensor using poly-(l-cysteine) functionalized CuO nanoneedles/N-doped reduced graphene oxide for detection of lead ions. *RSC Adv.* **2020**, *10*, 18526−18532.
(41) Elgrishi, N.; Rountree, K. J.; McCarthy, B. D.; Rountree, E. S.; Eisenhart, T. T.; Dempsey, J. L. A Practical Beginner's Guide to Cyclic Voltammetry. *J. Chem. Educ.* **2018**, *95*, 197−206.
(42) Aadil, M.; Shaheen, W.; Warsi, M. F.; Shahid, M.; Khan, M. A.; Ali, Z.; Haider, S.; Shakir, I. Superior electrochemical activity of α-Fe2O3/rGO nanocomposite for advance energy storage devices. *J. Alloys Compd.* **2016**, *689*, 648−654.
(43) Gao, E.; Wang, W. Role of graphene on the surface chemical reactions of BiPO4-rGO with low OH-related defects. *Nanoscale* **2013**, *5*, 11248−11256.
(44) Kumar, N. S.; Al-Ghurabi, E. H.; Asif, M.; Boumaza, M. Retrieving and morphological portrayal of Cu-nanoparticle impregnated reduced graphene oxide (CuNP@rGO) electrochemical biosensor. *Sens. Actuators, A* **2021**, *329*, No. 112826.
(45) Mandal, B. K.; Ogra, Y.; Suzuki, K. T. Identification of dimethylarsinous and monomethylarsonous acids in human urine of the arsenic-affected areas in West Bengal, India. *Chem. Res. Toxicol.* **2001**, *14*, 371−378.
(46) Wei, Y.; Gao, C.; Meng, F.; Li, H.; Wang, L.; Liu, J.; Huang, X. SnO_2/reduced graphene oxide nanocomposite for the simultaneous electrochemical detection of cadmium (II), lead(II), copper(II), and mercury(II): An interesting favorable mutual interference. *J. Phys. Chem. C* **2012**, *116*, 1034−1041.
(47) Kumar, R.; Bhuvana, T.; Sharma, A. Nickel tungstate-graphene nanocomposite for simultaneous electrochemical detection of heavy metal ions with application to complex aqueous media. *RSC Adv.* **2017**, *7*, 42146−42158.
(48) Li, L.; Liu, D.; Shi, A.; You, T. Simultaneous stripping determination of cadmium and lead ions based on the N-doped carbon quantum dots-graphene oxide hybrid. *Sens. Actuators, B* **2018**, *255*, 1762−1770.
(49) Xuan, X.; Park, J. Y. A miniaturized and flexible cadmium and lead ion detection sensor based on micro-patterned reduced graphene oxide/carbon nanotube/bismuth composite electrodes. *Sens. Actuators, B* **2018**, *255*, 1220−1227.
(50) Yukird, J.; Kongsittikul, P.; Qin, J.; Chailapakul, O.; Rodthongkum, N. ZnO@graphene nanocomposite modified electrode for sensitive and simultaneous detection of Cd (II) and Pb (II). *Synth. Met.* **2018**, *245*, 251−259.
(51) Priya, T.; Dhanalakshmi, N.; Thennarasu, S.; Karthikeyan, V.; Thinakaran, N. Ultra sensitive electrochemical detection of Cd^{2+} and Pb^{2+} using penetrable nature of graphene/gold nanoparticles/modified L-cysteine nanocomposite. *Chem. Phys. Lett.* **2019**, *731*, No. 136621.
(52) Nunes, E. W.; Silva, M.K.L.; Cesarino, I. Evaluation of a reduced graphene oxide-Sb nanoparticles electrochemical sensor for the detection of cadmium and lead in chamomile tea. *Chemosensors* **2020**, *8*, No. 53.
(53) Hou, X.; Xiong, B.; Wang, Y.; Wang, L.; Wang, H. Determination of trace lead and cadmium in decorative material using disposable screen- printed electrode electrically modified with reduced graphene oxide/L-cysteine/Bi-film. *Sensors* **2020**, *20*, No. 1322.
(54) Hao, Y.; Zhang, C.; Wang, W.; Wang, J.; Chen, S.; Xu, H.; Zhuiykov, S. Self-Assembled Co_3O_4/GO Composites for Excellent Electrochemical Detection of Heavy-Metal Ions. *J. Electrochem. Soc.* **2021**, *168*, No. 083503. https://orcid.org/0000-0003-0040-2539.
(55) Neralekere Somashekar, A. K.; Malingappa, P. Solvothermal synthesis of reduced graphene oxide and zinc ferrite containing composite and its application as an electrochemical sensor in simultaneous measurement of lead, cadmium and mercury ions. *J. Iran. Chem. Soc.* **2022**, *19*, 3481−3490.
(56) Li, Y.; Huang, H.; Cui, R.; Wang, D.; et al. Electrochemical sensor based on graphdiyne is effectively used to determine Cd^{2+} and Pb^{2+} in water. *Sens. Actuators, B* **2021**, *332*, No. 129519.
(57) Djebbi, M. A.; Allagui, L.; El Ayachi, M. S.; Boubakri, S.; Jaffrezic-Renault, N.; Namour, P.; Haj Amara, A. B. Zero-Valent Iron Nanoparticles Supported on Biomass-Derived Porous Carbon for Simultaneous Detection of Cd^{2+} and Pb^{2+}. *ACS Appl. Nano Mater.* **2022**, *5*, 546−558.
(58) Li, G.; Qi, X.; Zhang, G.; Wang, S.; Li, K.; Wu, J.; Wan, X.; Liu, Y.; Li, Q. Low-cost voltammetric sensors for robust determination of toxic Cd (II) and Pb(II) in environment and food based on shuttle-

like α-Fe_2O_3 nanoparticles decorated β-Bi_2O_3 microspheres. *Microchem. J.* **2022**, *179*, No. 107515.
(59) Li, G.; Qi, X.; Xiao, Y.; Zhao, Y.; Li, K.; Xia, Y.; Wan, X.; Wu, J.; Yang, C. An Efficient Voltammetric Sensor Based on Graphene Oxide-Decorated Binary Transition Metal Oxides Bi_2O_3/MnO_2 for Trace Determination of Lead Ions. *Nanomater.* **2022**, *12*, No. 3317.

https://doi.org/10.1021/acsomega.2c06080
ACS Omega 2022, 7, 45469−45480